IEEE Access
Multidisciplinary | Rapid Review | Open Access Journal

Received December 9, 2020, accepted January 4, 2021, date of publication January 8, 2021, date of current version January 14, 2021.

Digital Object Identifier 10.1109/ACCESS.2021.3049782

Optimized Tilt Fractional Order Cooperative Controllers for Preserving Frequency Stability in Renewable Energy-Based Power Systems

AHMED ELMELEGI[1], EMAD A. MOHAMED[1], MOKHTAR ALY[1,2], (Member, IEEE), EMAD M. AHMED[3,4], (Senior Member, IEEE), AL-ATTAR ALI MOHAMED[1], AND OSAMA ELBAKSAWI[3,5]

[1]Department of Electrical Engineering, Faculty of Engineering, Aswan University, Aswan 81542, Egypt
[2]Electronics Engineering Department, Universidad Tecnica Federico Santa Maria, Valparaiso 2390123, Chile
[3]Department of Electrical Engineering, Jouf University, College of Engineering, Sakaka 2014, Saudi Arabia
[4]AWCRC, Faculty of Engineering, Aswan University, Aswan 81542, Egypt
[5]Department of Electrical Engineering, Faculty of Engineering, Port-Said University, Port Said 42526, Egypt

Corresponding author: Emad A. Mohamed (emad.younis@aswu.edu.eg)

The authors extend their appreciation to the Deputyship for Research & Innovation, Ministry of Education in Saudi Arabia for funding this work through the project number ''375213500''. The authors also would like to extend their sincere appreciation to the central laboratory at Jouf University for support this study. This work is also supported in part by SERC Chile (ANID/FONDAP15110019) and by AC3E (ANID/Basal/FB0008).

ABSTRACT The low system inertia and the high sensitivity to load and generation fluctuations represent the main challenges for future ambitious plans of modern power systems accompanied by high penetrations levels of the renewable energy sources (RESs). Therefore, this article presents a new approach for solving the load frequency control (LFC) in addition to the virtual inertia control (VIC) in interconnected RESs penetrated power systems using cooperative tilt-based controllers and a hybrid modified particle swarm optimization with genetic algorithm (MPSOGA). The VIC system is adopted using superconducting magnetic energy storage (SMES) to provide sufficient inertial energy for system stability. Two tilt-based controllers are employed in each area using the tilt-integral-derivative (TID) controller for the SMES and TID with filter (TIDF) for the LFC function. The cooperative optimum design of the TID/TIDF controllers leads to the enhancement of frequency stability in studied two-area power systems. The formulated optimization process aims to minimize the frequency nadir settling time during abrupt changes of RESs and/or load changes, considering the cooperative control of LFC and VIC. The proposed approach has been applied to a case study consisting of two-area power systems, connected via hybrid high voltage DC/AC (hybrid HVAC/HVDC) tie-line, integrated with distributed conventional generations, photovoltaic (PV), and wind generation systems. Performance analysis has been conducted to demonstrate the effectiveness of the proposed method is compared to the genetic algorithm (GA) and particle-swarm optimization (PSO) using high fluctuations of renewable generations under extreme changes in loading conditions and physical parameters variation. The obtained results show the superiority of MPSOGA approach on the other competitive optimization techniques.

INDEX TERMS Hybrid optimization algorithm, interconnected power systems, load frequency control, renewable energy sources (RESs), superconducting magnetic energy storage (SMES), virtual inertia control.

I. INTRODUCTION

Promising strategic policies have been world-widely set for the expansion of using renewable energy sources (RESs) to compensate the continuously increasing population and the growing energy demands [1], [2]. High penetration levels of RESs have been achieved through wide installations of wind, solar photovoltaic (PV) and biomass energy, etc. Actually, power electronic conversion systems represent the main integration means for RESs with electrical power systems for achieving improved energy harvesting, power quality and energy efficiency for the RESs systems. However, the high

The associate editor coordinating the review of this manuscript and approving it for publication was Manoj Datta.

penetration levels of power electronic-based RESs cause significant reductions in the overall power system inertia [3], [4]. Several dangerous consequences and disturbances can be resulted due to the low inertia of high RESs penetration in the form of voltage and/or frequency fluctuations, instability of the power system, and possibility of successive interruptions in the power system operation. Thence, developing proper control systems and disturbance mitigation techniques are essential for enhancing future RESs-based power systems [5].

A wide employment of the virtual synchronous generator (VSG)-based control methods for solving the low inertia issues of RESs-based power systems are addressed in the literature [6]. The VSG control methods emulate the operation and performance of the classic synchronous generations without using prime movers. The VSG method has proven enhanced performance and stability of power system. From another side, the automatic load frequency control (ALFC) methods have achieved stable operation and proper control of the voltage and frequency during sudden load changes and generation/load imbalances. However, ALFC methods fail of mitigating fast frequency transients in power systems [7], [8].

Recently, several virtual inertia control (VIC) methods have been combined with ALFC methods for enhancing the frequency regulation [9]–[12]. The VIC methods have proven superior performance for mitigating the fast frequency transients. Among the various energy storage sources (ESSs), the superconducting magnetic energy storage (SMES) has been widely employed for VIC emulation, wherein improved system performance can be obtained [13], [14]. Several controllers have been widely employed for controlling VIC methods, such as the proportional-integral (PI) and proportional-integral-derivative (PID) strategies, fuzzy logic controller (FLC), model predictive control (MPC) [15], [16]. Additionally, more advanced and hybrid controllers using artificial intelligence were presented in the literature for controlling the load frequency. The coefficient diagram method (CDM) VIC has been presented in [17] for controlling VIC based single area power systems.

From another side, the robust control methods have been widely employed in the literature for the frequency regulation in power systems [18]. Robust stability and enhanced regulation has been achieved in these methods. However, these methods contain higher order controllers and their tuning processes are a cumbersome problem. The complexities in design and optimization processes of various controller parameters increases dramatically in multi-area interconnected power systems as direct result of the utilized high number of controllers [19]. The main objectives of the utilized controllers in the studied system are enhancing the frequency regulation of individual areas and controlling the tie-line power to support system stability.

In [3], a VIC system has been presented for the high voltage ac (HVAC) interconnected multi-area power systems at high penetration levels of RESs. Additionally, a derivative control method for VIC systems has been presented in [3] to preserve frequency stability with high voltage DC

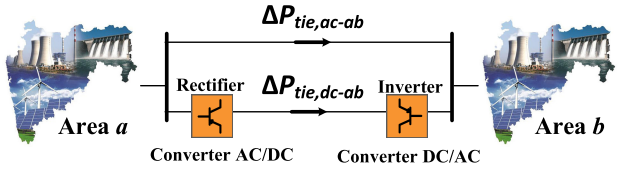

FIGURE 1. Schematic diagram of the electrical multi-area system using a hybrid HVAC/HVDC tie-line.

(HVDC) interconnected power system. In [20], an accurate modeling of HVDC tie-line was proposed for studying the automatic generation control (AGC)/LFC (AGC/LFC) of the multi-area power systems. The HVDC tie-line can perform the VIC functionality using the rectifier/inverter control at both sides. A similar approach has been presented in [21] by using fractional order control systems for the secondary frequency control side. However, the tuning process of the controller requires complex procedures in addition to the implementation complexities of the fractional order controller. Furthermore, distributed VIC systems for each area can provide better frequency stability performance and system reliability. Besides, a more complex controller design process is needed for the rectifier/inverter control to achieve multifunctionalities.

Lately, using tilt integral derivative controllers (TID) in load frequency control has been introduced [22]. The great advantageous in such controllers is implemented in their transfer function, which is being more similar to optimized one for achieving better feedback and reference tracking. The usefulness of using a derivative part in such controllers guarantees fast dynamic response for enhancing system stability [23]. Furthermore, fractional order controllers (FO) such as FO-based PID (FOPID) [24], fuzzy FO-based PI with PD controllers (FL-FOPI-FOPD) [25], fuzzy combined to FOPIDF (FL-FOPIDF) [26], combined fuzzy with PIDF in addition to FOI (FL-PIDF-FOI) [27], and hybrid FO-based control method [22] have been presented in the literature. FO controllers are exhibiting several merits due to their simplicity, robustness, and efficiency. However, the main challenge in using TID and FO controllers for LFC is being their high sensitivity to system uncertainties which is being the case in the modern power systems equipped with renewable energy sources. Therefore, it has become more crucial to the design process of the optimal controllers' parameters so as to have the capability to preserve system stability with any variations.

Several methods have been presented in the literature for solving the design problems of the control systems for frequency regulations for power systems. The analytical design methods suffer from the increased complexities due to adding the distributed VIC loops with the classical LFC loops. Additionally, several optimization algorithms have been employed in literature for tuning system controllers, such as the genetic algorithm (GA) [28], the particle-swarm optimization (PSO) [29], salp swarm algorithm (SSA) [30], artificial-bee colony

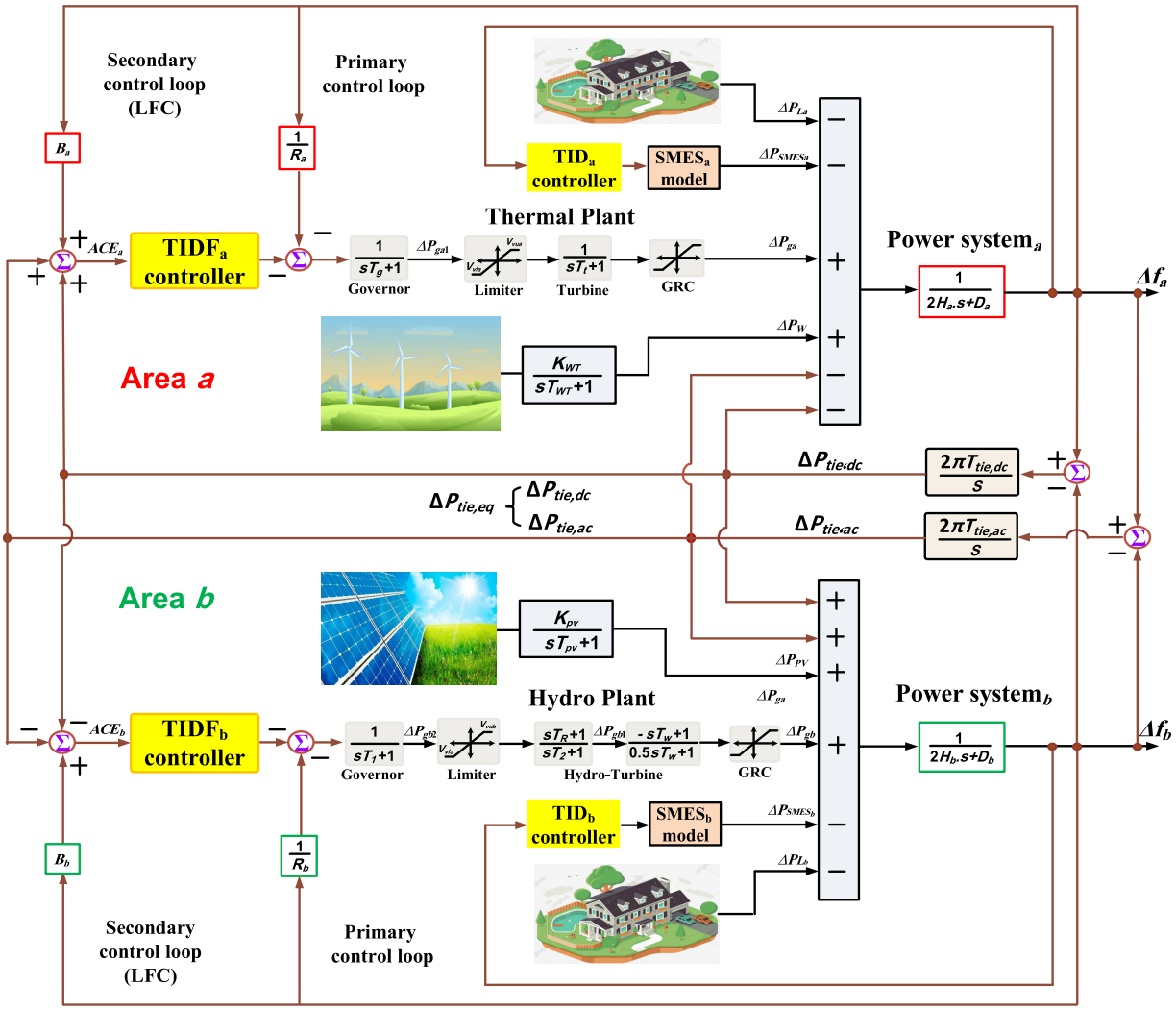

FIGURE 2. Dynamic model of the studied interconnected two-area electrical power system.

(ABC) [31], differential evolutions (DEs) [32], firefly algorithm (FA) [33], imperialist competitive algorithm (ICA) [34], whale optimization algorithm (WOA) [35], ant-lion optimizer algorithm (ALO) [36], and teaching learning based optimization (TLBO) [37], etc. However, the employment of distributed VIC loops in each of the interconnected areas with the existing LFC loops imposes several challenges for designing the controllers. In addition, the incorporation of the hybrid HVAC/HVDC tie-line would increase the system complexity and the controllers design process.

Therefore, from the above discussion, it has become clear that there are several issues and design challenges of controllers design in multi-area multi-sourced interconnected power systems. The challenges include the high number of controllers in each interconnected area in addition to the increased system complexity due to the employment of hybrid HVAC/HVDC tie-line. Therefore, the main contributions within this article are summarized as follows:

- Tilt-based controllers are presented in this article, including TIDF controller for LFC and TID for the SMES. The two controllers are designed optimally to achieve cooperative LFC and VIC for multi-area power systems.
- A hybrid MPSOGA method is presented in this article for the determining process of the optimum parameters for the two cooperative controllers in each area. The proposed MPSOGA technique provides enhanced coordination between the different controllers that result in power system stabilization and damping of the fluctuations due to the generation and/or load changes.
- A neighborhood search fully adjustable version of PSO, associative learning immediate memory mechanism is modified in terms of adaptive learning and information transfer rates to assist the exploitation ability and the fast convergence characteristics.
- In order to solve the current nonconvex nonlinear dynamic optimization problem, GA is integrated into

TABLE 1. Main parameters for the two-area power system ($x \in \{a, b\}$) [39].

Parameter	Symbol	Values	
		area a	area b
capacity rating	P_{rx} (MW)	1200	1200
Droop constant	R_x (Hz/MW)	2.4	2.4
Frequency bias value	B_x (MW/Hz)	0.4249	0.4249
Min. valve gate limit	V_{vlx} (p.u.MW)	-0.5	-0.5
Max. valve gate limit	V_{vux} (p.u.MW)	0.5	0.5
TC of thermal governor	T_g (s)	0.08	-
TC of thermal turbine	T_t (s)	0.3	-
TC of hydraulic governor	T_1 (s)	-	41.6
TC of Transient droop (hydraulic)	T_2 (s)	-	0.513
Reset time of hydraulic governor	T_R (s)	-	5
Water starting time of hydro turbine	T_w (s)	-	1
Power system inertia constant	H_x (p.u.s)	0.0833	0.0833
Power system damping coefficient	D_x (p.u./Hz)	0.00833	0.00833
TC of PV	T_{PV} (s)	-	1.3
Gain of PV	K_{PV} (s)	-	1
TC of wind	T_{WT} (s)	1.5	-
Gain of wind	K_{WT} (s)	1	-
TC of SMES converter	T_{DCx} (s)	0.03	0.03
coil of SMES	L_x (H)	0.03	0.03
SMES Control gain	K_{SMESx} (kV/unit MW)	100	100
Control gain	K_{Idx} (kV/kA)	0.2	0.2
Inductor rated current of SMES	I_{d0x} (kA)	4.5	4.5
capacity ratio of two-area system	A_{ab}	-1	
HVDC coefficient	$T_{tie,dc}$ (s)	0.1732	
HVAC coefficient	$T_{tie,ac}$ (s)	0.0865	

* TC denotes to time constant

the proposed paradigm to maintain the exploration over the course of generations, preventing a local optima premature convergence in the search space.

The remaining of this article is organized as following: Section II provides the structure of the multi-area multi-source interconnected power system, and the problem description of the current research. The system modelling of the studied system is introduced in Section III. Section IV provides the proposed MPSOGA method and the design platform of the optimized controllers. The simulation results for the designed system and the performance comparison of the proposed optimization platform with conventional design methods are provided in Section V. Finally, the conclusion of the paper is summarized in Section VI.

II. INTERCONNECTED POWER SYSTEM AND PROBLEM DESCRIPTION

A. INTERCONNECTED MULTI-AREA ELECTRICAL POWER SYSTEM

The electrical power systems are usually sectionalized into several individual power systems. However, the increased demand for bulk energy all over the world has directed the governments to interconnect the neighboring power systems via hybrid HVAC/HVDC tie-line [38]. Fig. 1 illustrates the schematic outline of the interconnected areas of electrical power system using hybrid HVAC/HVDC tie-line for exchanging power between the two-area. The interconnections among different areas are useful for reliability and economical issues, especially in case of generation unit failures. However, it is very difficult to preserve stability in a large multi-area network. This is due to that the existing large disturbances could propagate quickly via the whole system, which may lead to cascade tripping of units due to loss of system stability [20], [21].

Nonetheless, the multi-area power systems suffer from the limitations of increased penetration levels of RESs integration. The RESs are considered the main cause for the low power system inertia, which results in frequency and voltage instability problems. Thence, this article focuses on solving these challenges in multi-area systems to regulate and maintain their frequency stability. The case study is developed based on power system addressed in [39].

B. PROBLEM DESCRIPTION

The problem of designing and optimizing controller parameters in multi-area power systems arises from the increased number of controllers and their inherent dependencies on each other. In the selected case study, there are two-area electrical power system (area a) and (area b), which are connected via a hybrid HVAC/HVDC tie-line, and four different controllers that need to be optimized for enhancing the rendering of the interconnected power system. Moreover, the utilization of distributed RESs between the two-area with the employment of hybrid HVAC and HVDC tie-lines are also beholded in the proposed case study. The main objectives of the designed controllers are to regulate the local system frequency at each area and to regulate the hybrid HVAC/HVDC tie-line power flows among neighboring areas. The foregoing controllers, as discussed in the above section, suffer from increased fluctuations, and decreased robustness under the effects of system disturbances, increased penetration levels of RESs, and tie-line failures.

The overall modelling of the presented electrical two-area power system and the connected supply/loads are shown in Fig. 2. TID controllers are used for the SMES and TID with filter (TIDF) are used for the secondary LFC in the studied electrical system. The regulation of the system frequency is enhanced through the formulated co-optimized process for the parameters of the utilized cooperative optimum design of the TID/TIDF controllers. The regulation includes any sudden changes for frequency deviations in area a (Δf_a) and area b (Δf_b) in addition to the deviations in tie-line power between the two-area ($\Delta P_{tie,eq}$), which includes the HVAC tie-line power ($\Delta P_{tie,ac}$) and the HVDC tie-line power ($\Delta P_{tie,dc}$). This cooperative optimization has the ability to find the sub-optimal solutions for the whole cooperative system under different cases of disturbances with an increased penetration level of RESs.

III. SYSTEM MODELLING

The first step in the controller design and the optimization process is modelling and determining the various parameters and elements in the selected studied system. This section presents the main components and their corresponding mathematical representation for the selected case study

A. CASE STUDY OF THE INTERCONNECTED TWO-AREA POWER SYSTEM

In the studied system, a thermal power plant and wind power generation are included in area a, while area b consists of a hydraulic power plant and PV generators. Both areas include SMES storage systems and different types of loads. The parameters of the studied interconnected two-area electrical power system are listed in Table. 1 [39].

B. DYNAMIC MODELLING OF THE GENERATION SYSTEM

The generation units in the two-area consists of conventional thermal power plant, hydraulic power plant, wind power generation, and PV generator. The thermal power plant turbine $G_t(s)$ and governor $G_g(s)$ can be represented by their transfer functions (TF) as follows:

$$G_g(s) = \frac{1}{T_g s + 1} \tag{1}$$

$$G_t(s) = \frac{1}{T_t s + 1} \tag{2}$$

The hydro turbine TF is composed of speed governor, droop compensation and the penstock turbine. The hydro turbine is modelled as follows [40]:

$$G_h(s) = \frac{1}{T_1 s + 1} \cdot \frac{T_R s + 1}{T_2 s + 1} \cdot \frac{-T_w s + 1}{0.5 T_w s + 1} \tag{3}$$

whereas, the TF modeling of the power system $G_{px}(s)$ is modeled as:

$$G_{px}(s) = \frac{1}{2H_x s + D_x} \tag{4}$$

The TF of the wind unit $G_{WT}(s)$ and the PV unit $G_{PV}(s)$ are modelled as follows:

$$G_{WT}(s) = \frac{K_{WT}}{T_{WT} s + 1} \tag{5}$$

$$G_{PV}(s) = \frac{K_{PV}}{T_{PV} s + 1} \tag{6}$$

A complete system model is constructed by combining the various aforementioned models. The state-space modeling is constructed for the system. In the presented state-space modeling, x, y, ω and u are the vectors for representing the state variables, the output states, the disturbances, and other control variables, respectively. In the studied system, the considered control variables include ACE signals in each area (ACE_a and ACE_b), SMES output power difference in each area (ΔP_{SMES_a} and ΔP_{SMES_b}). Whereas, A, B_1, B_2, and C are the parameters matrices that correspond to the linearized state-space modeling of the studied system. The state space modelling and its parameters are expressed as follows:

$$\dot{x} = Ax + B_1\omega + B_2 u \tag{7}$$

$$y = Cx \tag{8}$$

C. MODELLING OF THE SMES SYSTEM

In the studied system, SMES is selected among the various types of ESSs as VIC device for mitigating the fast deviations in the areas frequencies due to its merits of fast response, long lifetime operation, and high efficiency compared to the other existing ESSs [41]. The power conversion system of the SMES is including three-phase transformer, voltage source converter (VSC) and dc-link capacitor as shown in Fig. 3a. During the normal conditions, SMES is charging through the power grid and is kept ready to compensate any system fluctuations. Whenever system disturbances occurred, SMES discharging starts through the power condition unit to restore power system equilibrium and maintain system balancing [42]. SMES is modeled as a linearized first order model to be more appropriate in LFC as shown in Fig. 3b.

The frequency deviations Δf_a and Δf_b with using hybrid HVAC/HVDC tie-line with controlling the distributed SMES systems in area a and area b can be obtained as follows:

$$\Delta f_a = \frac{1}{2H_a s + D_a}[\,\Delta P_{m_a} + \Delta P_{W_a} - \Delta P_{L_a} - \Delta P_{SMES_a} - \Delta P_{tie,eq}] \tag{15}$$

$$\Delta f_b = \frac{1}{2H_b s + D_b}[\,\Delta P_{m_b} + \Delta P_{PV_b} - \Delta P_{L_b} - \Delta P_{SMES_b} - A_{ab}\ \Delta P_{tie,eq}] \tag{16}$$

whereas, $\Delta P_{tie,eq}$ represents the tie-line power flow between the two-areas and its model is provided in Section III-D.

D. MODELLING OF THE HYBRID HVAC/HVDC TIE-LINE SYSTEM

In the studied system, the configuration of hybrid HVAC/HVDC tie-line is used for connecting the two-area,

as shown in Fig. 1. The hybrid HVAC/HVDC tie-line configuration is employed due to its ability to enhance performance of the AC system dynamics [20]. The equivalent two-area model equipped with hybrid HVAC/HVDC tie-line is depicted in Fig. 4. It is seen that the HVDC system can be modelled as a series composition of two voltage sources E_a, E_b and their corresponding phase angles are γ_a, γ_b, respectively. The HVDC tie-line can be modelled as two impedance phase reactors X_a, X_b for each connection side. The transferred power from area a to area b through the HVDC tie-line is represented as following:

$$P_{tie,dc\_ab} = \frac{V_a * E_a}{X_a} \sin(\delta_a - \gamma_a) \tag{17}$$

where, P_{tie,dc_ab} is the transferred power from area a to area b through the HVDC tie-line. By linearizing (17), it gives

$$\Delta P_{tie,dc\_ab} = T_{tie,dc\_ab} (\Delta\delta_a - \Delta\gamma_a) \tag{18}$$

$$x = \left[\Delta f_a\ \Delta P_{ga}\ \Delta P_{ga1}\ \Delta P_{WT}\ \Delta f_b\ \Delta P_{gb}\ \Delta P_{gb1}\ \Delta P_{gb2}\ \Delta P_{PV}\ \Delta P_{tie,eq}\right]^T \tag{9}$$

$$\omega = \left[\Delta P_{la}\ P_{WT}\ \Delta P_{lb}\ P_{PV}\right]^T \tag{10}$$

$$u = \left[ACE_a\ \Delta P_{SMES_a}\ ACE_b\ \Delta P_{SMES_b}\right]^T \tag{11}$$

$$A = \begin{bmatrix}
-\frac{D_a}{2H_a} & \frac{1}{2H_a} & 0 & \frac{1}{2H_a} & 0 & 0 & 0 & 0 & 0 & -\frac{1}{2H_a} \\
0 & -\frac{1}{T_t} & \frac{1}{T_t} & 0 & 0 & 0 & 0 & 0 & 0 & 0 \\
-\frac{1}{R_a T_g} & 0 & -\frac{1}{T_g} & 0 & 0 & 0 & 0 & 0 & 0 & 0 \\
0 & 0 & 0 & -\frac{1}{T_{WT}} & 0 & 0 & 0 & 0 & 0 & 0 \\
0 & 0 & 0 & 0 & -\frac{D_b}{2H_b} & \frac{1}{2H_b} & 0 & 0 & \frac{1}{2H_b} & \frac{1}{2H_b} \\
0 & 0 & 0 & 0 & \frac{2T_R}{R_b T_1 T_2} & -\frac{2}{T_w} & \frac{2T_2+2T_w}{T_2 T_w} & \frac{2T_R-2T_1}{T_1 T_2} & 0 & 0 \\
0 & 0 & 0 & 0 & -\frac{T_R}{R_b T_1 T_2} & 0 & -\frac{1}{T_2} & \frac{T_1-T_R}{T_1 T_2} & 0 & 0 \\
0 & 0 & 0 & 0 & -\frac{1}{R_b T_1} & 0 & 0 & -\frac{1}{T_1} & 0 & 0 \\
0 & 0 & 0 & 0 & 0 & 0 & 0 & 0 & -\frac{1}{T_{PV}} & 0 \\
2\pi T_{tie,eq} & 0 & 0 & 0 & -2\pi T_{tie,eq} & 0 & 0 & 0 & 0 & 0
\end{bmatrix} \tag{12}$$

$$B_1 = \begin{bmatrix}
-\frac{1}{2H_a} & 0 & 0 & 0 \\
0 & 0 & 0 & 0 \\
0 & 0 & 0 & 0 \\
0 & \frac{K_{WT}}{T_{WT}} & 0 & 0 \\
0 & 0 & -\frac{1}{2H_b} & 0 \\
0 & 0 & 0 & 0 \\
0 & 0 & 0 & 0 \\
0 & 0 & 0 & 0 \\
0 & 0 & 0 & \frac{K_{PV}}{T_{PV}} \\
0 & 0 & 0 & 0
\end{bmatrix}, \text{ and } \quad B_2 = \begin{bmatrix}
0 & -\frac{1}{2H_a} & 0 & 0 \\
0 & 0 & 0 & 0 \\
-\frac{1}{T_g} & 0 & 0 & 0 \\
0 & 0 & 0 & 0 \\
0 & 0 & 0 & -\frac{1}{2H_b} \\
0 & 0 & \frac{2T_R}{T_1 T_2} & 0 \\
0 & 0 & -\frac{T_R}{T_1 T_2} & 0 \\
0 & 0 & -\frac{1}{T_1} & 0 \\
0 & 0 & 0 & 0 \\
0 & 0 & 0 & 0
\end{bmatrix} \tag{13}$$

$$C = \begin{bmatrix}
1 & 0 & 0 & 0 & 0 & 0 & 0 & 0 & 0 & 0 \\
B_a & 0 & 0 & 0 & 0 & 0 & 0 & 0 & 0 & 1 \\
0 & 0 & 0 & 0 & 1 & 0 & 0 & 0 & 0 & 0 \\
0 & 0 & 0 & 0 & B_b & 0 & 0 & 0 & 0 & -1
\end{bmatrix} \tag{14}$$

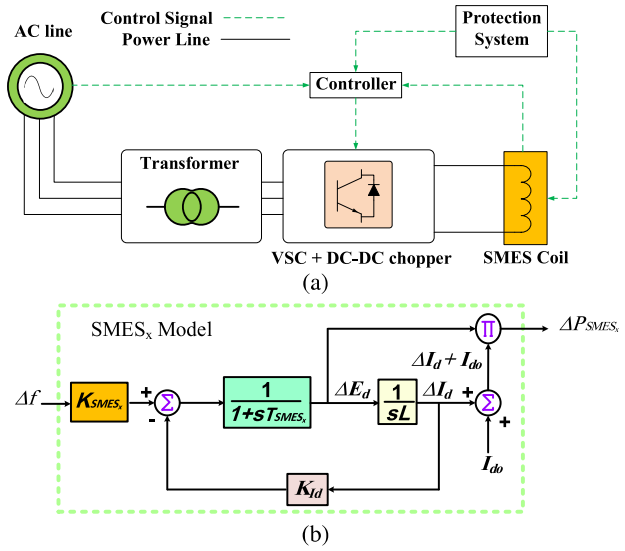

FIGURE 3. SMES-based VIC system: (a) The components of SMES power conversion system, and (b) The dynamic model of SMES for VIC function.

where T_{tie,dc_ab} represents the converter AC/DC synchronizing coefficient and it is given by:

$$T_{tie,dc\_ab} = \frac{V_a * E_a}{X_a} \cos(\delta_a^0 - \gamma_a^0) \tag{19}$$

For area b, P_{tie,dc_ba} represents the transferred power from area b to area a through the HVDC tie-line. Then, $\Delta P_{tie,dc\_ba}$ can be obtained as follows:

$$\Delta P_{tie,dc\_ba} = T_{tie,dc\_ba}\,(\Delta\delta_b - \Delta\gamma_b) \tag{20}$$

where T_{tie,dc_ba} represents the converter DC/AC synchronizing coefficient and it is given by:

$$T_{tie,dc\_ba} = \frac{V_b * E_b}{X_b} \cos(\delta_b^0 - \gamma_b^0) \tag{21}$$

During load changes, (18) and (20) constitute the deviations of tie-power of the HVDC tie-line between the two-area. The transferred power between the two-area after ignoring the tie-line power losses can be represented as follows:

$$\Delta P_{tie,dc\_ab} = -\Delta P_{tie,dc\_ba} \tag{22}$$

Substituting (22) into (18) and (20), it becomes as follows:

$$T_{tie,dc\_ab}\,(\Delta\delta_a - \Delta\gamma_a) = -T_{tie,dc\_ba}\,(\Delta\delta_b - \Delta\gamma_b) \tag{23}$$

The power transferred between the DC/AC power converter and the AC/DC power converter in the two-area via the HVDC tie-line in both sides are equal. This in turn requires that the the change in phase angle $\Delta\gamma_a$ of AC/DC converter and the change in phase angle $\Delta\gamma_b$ of DC/AC converter are related as follows:

$$\Delta\gamma_a = \Delta\gamma_b = \Delta\gamma \tag{24}$$

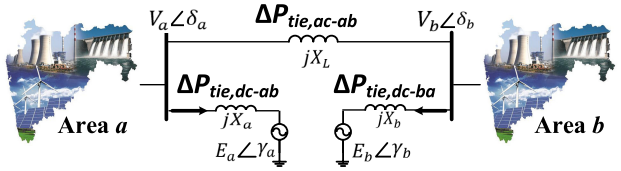

FIGURE 4. The equivalent hybrid HVAC/HVDC tie-line model.

Substituting (24) in (23)

$$\Delta\gamma = \frac{\Delta\delta_a + (\frac{T_{tie,dc\_ba}}{T_{tie,dc\_ab}})\,\Delta\delta_b}{1 + \frac{T_{tie,dc\_ba}}{T_{tie,dc\_ab}}} \tag{25}$$

In addition, substituting (24) in (18) gives

$$\Delta P_{tie,dc\_ab} = \frac{T_{tie,dc\_ab}\,T_{tie,dc\_ba}}{T_{tie,dc\_ab} + T_{tie,dc\_ba}}\,(\Delta\delta_a - \Delta\delta_b) \tag{26}$$

where, T_{tie,dc_ab} is the tie-line synchronizing coefficient between the two-area a and b, and it is defined as follows [20]:

$$\Delta P_{tie,dc\_ab} = 2\pi\ T_{tie,dc\_ab} \int (\Delta f_a - \Delta f_b)\,dt \tag{27}$$

Then, (27) becomes as follows:

$$\Delta P_{tie,dc\_ab} = 2\pi\ \frac{T_{tie,dc\_ab}\,T_{tie,dc\_ba}}{T_{tie,dc\_ab} + T_{tie,dc\_ba}} \int (\Delta f_a - \Delta f_b)\,dt \tag{28}$$

Afterwards, the Laplace transform for (28) is performed as follows:

$$\Delta P_{tie,dc\_ab}(s) = 2\pi\ \frac{T_{tie,eq}}{s}\,(\Delta f_a(s) - \Delta f_b(s)) \tag{29}$$

whereas, the equivalent HVDC synchronization coefficient can be determined as follows:

$$T_{tie,eq} = \frac{(T_{tie,dc\_ab}\,T_{tie,dc\_ba})}{(T_{tie,dc\_ab} + T_{tie,dc\_ba})} \tag{30}$$

IV. PROPOSED METHOD

A. THE PROPOSED TILT-BASED CONTROLLERS

Recently, advanced applications and utilization of fractional order based control systems are presented in [39], [43]. They have proven robust and high performance control of various systems. By employing the fractional type of integrators and/or differentiators, more design flexibility for the control system is achieved. Generally, the representation of fractional order operators is obtained by ${}_{t_0}D_{t_f}^{\alpha}$, where, t_0 and t_f denote to time limits of the calculation process of operators, and α represents the order of the operator [44]. The fractional-order operators take various forms as follows:

$${}_{t_0}D_{t_f}^{\alpha} = \begin{cases} \alpha > 0 \ \rightarrow \ \dfrac{d^{\alpha}}{dt^{\alpha}} \\ \alpha < 0 \ \rightarrow \ \int_{t_0}^{t_f} dt^{\alpha} \\ \alpha = 0 \ \rightarrow \ 1 \end{cases} \tag{31}$$

whereas, several methods are applied in literature for the definition and approximation of fractional operators [43], [45]. Among these methods, Oustaloup approximate representation of fraction operators have found wide employment and it will be used in this article. In which, the band passing filter is designed in certain range of frequency $[\omega_{\text{fbl}}, \omega_{\text{fbu}}]$, where ω_{fbl} and ω_{fbu} denote the lower, and the upper values for frequency limits, respectively. The approximated transfer function representation for s^{λ} ($\lambda \in \Re$) is represented by the integer order based equivalent transfer function with its gains, poles, and zeros are expressed as follows [44]:

$$s^{\lambda} \approx K \prod_{k=-M}^{M} \frac{s+\omega_{\text{k}}^{\text{z}}}{s+\omega_{\text{k}}^{\text{p}}} \tag{32}$$

$$\omega_{\text{k}}^{\text{z}} = \omega_{\text{fbl}} \left(\frac{\omega_{\text{fbu}}}{\omega_{\text{fbl}}}\right)^{\frac{k+M+\frac{1-\lambda}{2}}{2M+1}} \tag{33}$$

$$\omega_{\text{k}}^{\text{p}} = \omega_{\text{fbl}} \left(\frac{\omega_{\text{fbu}}}{\omega_{\text{fbl}}}\right)^{\frac{k+M+\frac{1+\lambda}{2}}{2M+1}} \tag{34}$$

$$K = \left(\frac{\omega_{\text{fbu}}}{\omega_{\text{fbl}}}\right)^{\frac{-\lambda}{2}} \prod_{k=-M}^{M} \frac{\omega_{\text{k}}^{\text{p}}}{\omega_{\text{k}}^{\text{z}}} \tag{35}$$

where, $\omega_{\text{k}}^{\text{p}}$ and $\omega_{\text{k}}^{\text{z}}$ denote to poles, and the zeros for the sequence k. Wheres, approximate transfer function for the operator has the $(2M + 1)$ numbers of the poles/zeros. The present study considers that the selected order for the Oustaloup method ($M = 5$) with the frequency range in $\omega \in [\omega_{\text{fbl}}, \omega_{\text{fbu}}]$ in range between $[-1000, 1000]$ rad/s.

In the literature, the PID integral based controllers are used in several applications due to their simplicity in the design process. The PID controllers can be expresses as follows:

$$C(s) = \frac{Y(s)}{E(s)} = K_p + \frac{K_i}{s} + K_d\, s \tag{36}$$

where, K_p, K_i and K_d denote to the proportional, the integral and the differential gains for PID controller. Whereas, the fractional order types of PID (FO-PID) control can be expressed as follows:

$$C(s) = \frac{Y(s)}{E(s)} = K_p + \frac{K_i}{s^{\lambda}} + K_d\, s^{\mu} \tag{37}$$

where, μ, and λ are the FO operators and their tuning ranges lie between $[0, 1]$.

Due to the robust and improved performance of applying the fractional order control systems, they are selected for the proposed controller. In each area, tilt-integral-derivative (TID) based controller are utilized in the SMES controller. The TID controller is expressed as following:

$$C(s) = \frac{Y(s)}{E(s)} = K_t\, s^{-(\frac{1}{n})} + \frac{K_i}{s} + K_d\, s \tag{38}$$

where, n is the tilt fractional component. This component is advantageous at providing more simplified tuning process, enhanced disturbance rejection ability, and improved robustness against the parameters uncertainty. Whereas, the TID with filter (TIDF) is selected for controlling the LFC in each area. The TIDF controller is operated in a cooperative way with the TID of the VIC controller, and their tuning process is made simultaneously. The TIDF controller is expressed as follows:

$$C(s) = \frac{Y(s)}{E(s)} = K_t\, s^{-(\frac{1}{n})} + \frac{K_i}{s} + K_d\, \frac{N_c s}{s+N_c} \tag{39}$$

where, N_c is the coefficient of derivative filter of TIDF controller. Fig. 5 presents the schematic diagram for the proposed cooperative controller. It has become clear that each area has 4 tunable parameters in the TID controller in addition to the 5 tunable parameters in the TIDF controller. Therefore, there are total of 9 parameters that need to be tuned in each area that lead to total of 18 parameters for the selected two-area power systems. In the following subsections, the proposed optimization algorithm is presented for simultaneous tuning process for the proposed controllers.

B. THE PROPOSED HYBRID MODIFIED PSO AND GA APPROACH

The above formulated problem of the optimal controller parameters for the considered two-area power systems is a dynamic nonlinear optimization problem. For solving such problem, a fast convergence and efficient search method is needed. In that respect, the proposed paradigm aims to integrate the advantages of high exploration ability of genetic algorithm (GA) with the exploitation feature of the modified version of particle-swarm optimization (PSO) in form of the associative learning immediate memory technique to improve the neighborhood search, thereby decreasing the search space, according to the following steps as shown in Fig. 6.

1) INITIALIZATION

For dimensional (d) and population number (n), the population positions are randomly generated as follows:

$$x_{ij} = rand[0, 1] \cdot (x_j^{max} - x_j^{min}) + x_j^{min}, \quad \forall\, i \in \{,, 2, .., n\},\ j \in \{,, 2, .., d\} \tag{40}$$

where, x_j^{max} and x_j^{min} represent the upper limit and the lower limit, respectively. The initial population is divided into two equal halves according to their determined fitness. In GA phase, the better half of the population is selected as parents under natural selection of 0.5 to generate children population as positions of the worse half. The mating vectors resulting from the GA phase are used in the following MPSO phase with the aid of associative learning immediate memory mechanism to update positions of the better half of the population.

2) GENETIC PHASE

For increasing the efficiency of the optimization process and preventing early convergence, the GA operators (i.e., crossover in addition to mutation operators) are applied for enhancing the solution diversity, discovering the whole searching area. In any next step after the initialization, better

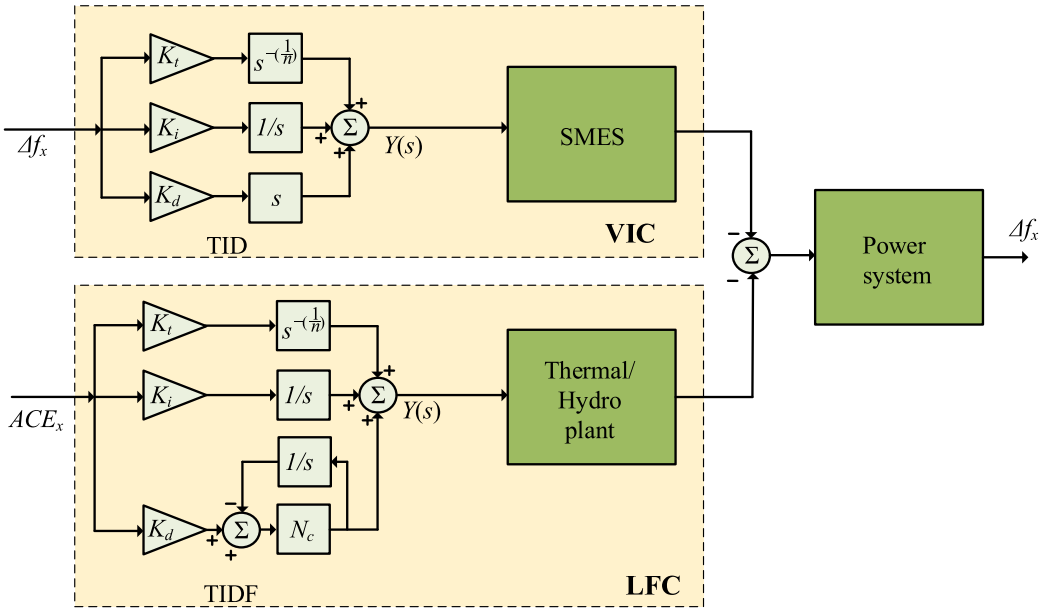

FIGURE 5. The proposed TID/TIDF cooperative controller for each area.

individuals, who were discovered after population sorting according to their fitness, are considered elite individuals and are employed as candidate parents. At least one descendant is generated from each pair of candidate parents, which are selected randomly from better individuals. The size of the worse population manipulate under 0.05 mutation rate is $n_{ch} = floor(n/2)$, where elite individuals size is $n_e = n - n_{ch}$. Parents' vectors share their tails that produce randomly from a single crossover point to generate new offspring. It should be noted that the use of elite individuals leads to some exploitation in this exploration stage, which ensures that better control variables are replicated in the following iterations. The fitness of offspring $f(x_{ch}^{(t+1)})$ are calculated and compared with their old positions $f(x_{ch}^{t})$ using survival of the fittest strategy that can be formulated for this minimization problem using the following equation.

$$x_{ch}^{t+1} = \begin{cases} x_{ch}^{t}, & \text{if } f(x_{ch}^{(t+1)}) \geq f(x_{ch}^{(t)}) \\ x_{ch}^{t+1}, & \text{if } f(x_{ch}^{(t+1)}) < f(x_{ch}^{(t)}) \end{cases} \quad \forall\, ch \in \{, , 2, .., n_{ch}\} \tag{41}$$

At the end of this stage, number of mating vectors are identified, using probability distribution function, from the entire population for use as a guide for the next stage.

3) ASSOCIATIVE LEARNING PHASE

The mating/guidance vectors are selected to update the positions of elite individuals. Therefore, the best individuals $(x_i^{(t+1))}$ are assigned to drift towards promising areas that emerge through mating vectors using the following associative learning immediate memory (ALIM) [46], [47].

$$\begin{aligned} & x_i^{t+1} \\ & = x_i^t + 0.05 \cdot (1 - \frac{t}{T}) \cdot G[x_i^t - x_i^{min}, x_i^{max} - x_i^t] \\ & \quad + (2 - \frac{2t}{T}) \cdot r_1 \cdot (bestp^t - x_i^t) + \frac{t}{T} \cdot r_2 \cdot (bestg^t - x_i^t) \\ & \quad \forall\, i \in \{, , 2, .., n_e\} \end{aligned} \tag{42}$$

where, t denotes to the generation number, T represents the maximum generations number, G is the Gaussian distribution, r_1 and r_2 denote to the random number within $[0, 1]$, $best_p$ is is a guidance vector identified by the probability distribution, $best_g$ is the global solution, $2 - 2t/T$ is the cognitive factor, and t/T is the social factor. It should be noted that despite the increase in intergenerational transmission information to 0.05, the cognitive factor increased by twice and the social factor decreased by half [1, 2] in order to improve the exploration ability in this exploitation phase, the convergence speed remains high with the improvement of local research provided by the global solution and guidance vectors. Source of the implemented codes by the authors and used for the experiments are freely available at [48].

C. THE PROPOSED DESIGN APPROACH

1) THE SELECTION OF OBJECTIVE FUNCTION

The proposed control strategy is based on a cooperative control of the VIC based-SMES device and the LFC method. The TIDF controller is used as the secondary control method for area a in addition to area b, and the TID controller is employed for the VIC of $(SMES_a)$ and $(SMES_b)$ as shown in Fig. 2. The input signals to the proposed controllers are the frequency deviations of area a using (Δf_a) signal and of area b using (Δf_b) signal. The controllers TID controllers

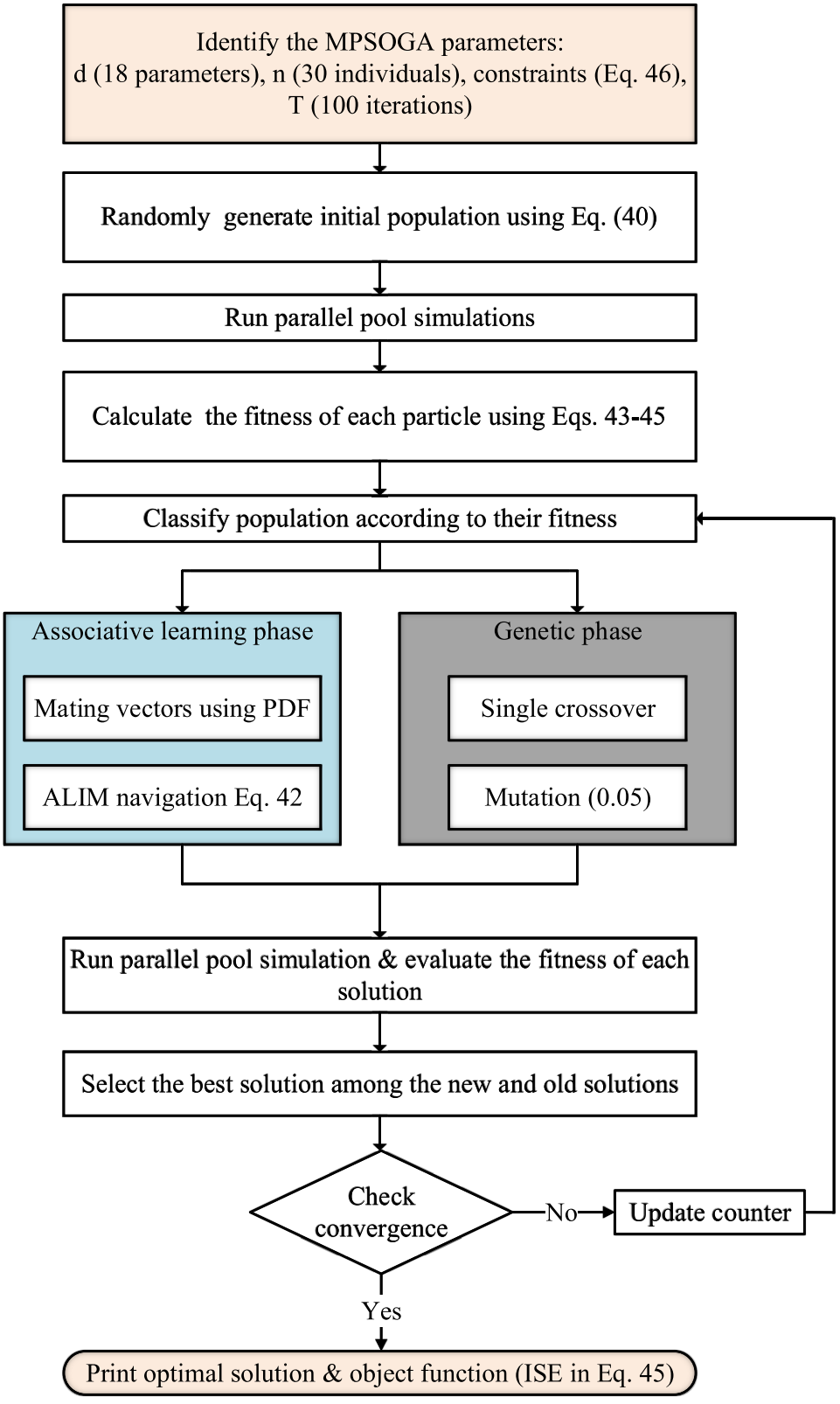

FIGURE 6. The proposed implementation of the MPSOGA-TID/TIDF cooperative controller.

are utilized for the SMES to achieve a desired performance objectives and to reject the various disturbances. Whereas, TID controllers are employed for the the area control error (ACE) for area a (ACE_a) and for area b (ACE_b), respectively. Fig. 5 shows the proposed cooperative control method. The area control errors of the two-area can be represented as

follows:

$$ACE_a = \Delta P_{tie,ac} + \Delta P_{tie,dc} + B_a\ \Delta f_a \quad (43)$$

$$ACE_b = A_{ab}\ \Delta P_{tie,ac} + A_{ab}\ \Delta P_{tie,dc} + B_b\ \Delta f_b \quad (44)$$

where,(A_{ab}) is considered two-area capacity ratio.

There are several error-based objective functions for multi-objective control systems, such as: the integral-squared error (ISE), the integral time-squared error (ITSE), and the integral-time absolute error (ITAE), etc. The ISE is selected in this article for representing the objective function. The main benefits behind the preference of the ISE over the other time-based methods (ITSE and ITAE) are the more penalization of the large error due to using larger squared values, and their ability to reduce peak frequency deviations. Thence, the ISE is selected in this work for optimizing the control objectives of the cooperative VIC and LFC systems. In the selected system, the four proposed controllers are tuned by a novel intelligent searching algorithm based on the proposed MPSOGA algorithm. The transfer function of the TIDF controllers for the LFC in the two-area are $G_1(s)$ and $G_2(s)$, where ($G1_(s) = K_{t1}s^{-1/n_1} + \frac{K_{i1}}{s} + K_{d1}\ \frac{N_{c1}s}{s+N_{c1}}$ and $G2_(s) = K_{t2}s^{-1/n_2} + \frac{K_{i2}}{s} + K_{d2}\ \frac{N_{c2}s}{s+N_{c2}}$) requires the determination of five optimal parameters in each area (total of 10 in the two-area) that are ($K_{t1}, K_{t2}, K_{i1}, K_{i2}, K_{d1}, K_{d2}, n_1, n_2, N_{C1}, N_{c2}$). Whereas, the transfer function of the TID controllers for the LFC in the two-area are $G_3(s)$ and $G_2(s)$, where ($G3_(s) = K_{t3}s^{-1/n_3} + \frac{K_{i3}}{s} + K_{d3}\ \ s$ and $G4_(s) = K_{t4}s^{-1/n_4} + \frac{K_{i4}}{s} + K_{d4}\ \ s$) requires the determination of four optimal parameters in each area (total of 8 in the two-area) that are ($K_{t3}, K_{t4}, K_{i3}, K_{i4}, K_{d3}, K_{d4}, n_3, n_4$). Therefore, the proposed optimization method has to determine the optimum values for the 18 parameters for the case study.

The fitness function of the ISE in the proposed control system has to maintain the frequency deviation in area a (Δf_a) and in area b (Δf_b) in the two-area and the HVDC tie-line ($\Delta P_{tie,dc}$) in addition to HVAC tie-line power ($\Delta P_{tie,ac}$) to a minimum value. The selected objective function in the proposed optimization technique is expressed as follows:

$$ISE = \int_0^{t_s} \{(\Delta f_a)^2 + (\Delta f_b)^2 + (\Delta P_{tie,dc})^2 + (\Delta P_{tie,ac})^2\} \quad (45)$$

2) THE CONSTRAINT OF PROPOSED OPTIMIZATION

The aforementioned 10 parameters of the TIDF and TID in both areas represent the constrains of the proposed optimization task. These parameters are bounded in the optimization process by certain predefined limits. The ranges of such parameters are defined as follows:

$$\begin{aligned} K_t^{min} &\le K_{t1}, K_{t2}, K_{t3}, K_{t4} \le K_p^{max} \\ K_i^{min} &\le K_{i1}, K_{i2}, K_{i3}, K_{i4} \le K_i^{max} \\ K_d^{min} &\le K_{d1}, K_{d2}, K_{d3}, K_{d4} \le K_d^{max} \\ n^{min} &\le n_1, n_2, n_3, n_4 \le n^{max} \\ N_c^{min} &\le N_{c1}, N_{c2} \le N_c^{max} \end{aligned} \quad (46)$$

TABLE 2. Optimal coefficients for the selected case study.

Algorithm	Controller	Coefficients				
		K_t	K_i	K_d	n	N_c
MPSOGA	TID_a	1.9764	1.9432	1.9161	2.92	-
	$TIDF_a$	1.9197	1.9073	1.8759	3.23	4.861
	TID_b	1.8829	1.4249	1.7542	2.85	-
	$TIDF_b$	0.7919	1.6101	1.2454	3.05	351.93
GA	TID_a	1.9804	1.9565	1.4153	2.63	-
	$TIDF_a$	1.9944	1.5528	1.3012	2.45	253.9
	TID_b	1.8252	1.5754	1.2404	2.24	-
	$TIDF_b$	0.7553	0.3534	1.1909	2.61	312.53
PSO	TID_a	1.5196	1.9637	1.3174	2.55	-
	$TIDF_a$	0.8386	1.9844	1.7209	4.01	273.55
	TID_b	1.8412	0.3585	0.2925	4.67	-
	$TIDF_b$	0.8009	0.9946	0.4801	3.94	257.62

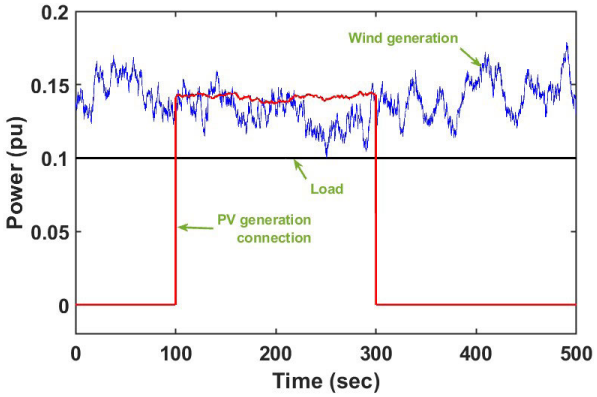

FIGURE 7. Generation profile for scenario 1.

where, $(f)^{min}$ and $(f)^{max}$ denote to minimum and maximum limits of the parameters in the proposed controller. In the selected case study, all the minimum values of K_t^{min}, K_i^{min}, K_d^{min} are selected to be zero, while the maximum values of K_t^{max}, K_i^{max}, K_d^{max} are selected to be 20. Moreover, n^{min} and n^{max} limits are selected to be 1 and 10, respectively. in addition, N_c^{min} and N_c^{max} limits are selected to be 1 and 500, respectively.

V. SIMULATION RESULTS AND PERFORMANCE VERIFICATION

Throughout this section, the proposed cooperative VIC (SMES based-TID), LFC based-TIDF controllers and the proposed MPSOGA optimization technique are validated through using the simulation results of MATLAB/Simulink software. Table. 2 summarizes the designed gains of the proposed controllers using the proposed MPSOGA algorithm and some selected conventional optimization methods.

A. SCENARIO 1: BEHAVIOR OF RESs

In this scenario, the performance of the studied system with the proposed cooperative control is tested under the influence of the fluctuated nature of the RESs. A high fluctuated wind power of 0.18 p.u. is installed in area a, while a solar generation system with peak of 0.148 p.u. is installed in area b. In this scenario, the PV generation in area b is connected at time $t = 100$ s with gradual increase to emulate the nature of PV systems. Then, the PV generation is disconnected at time

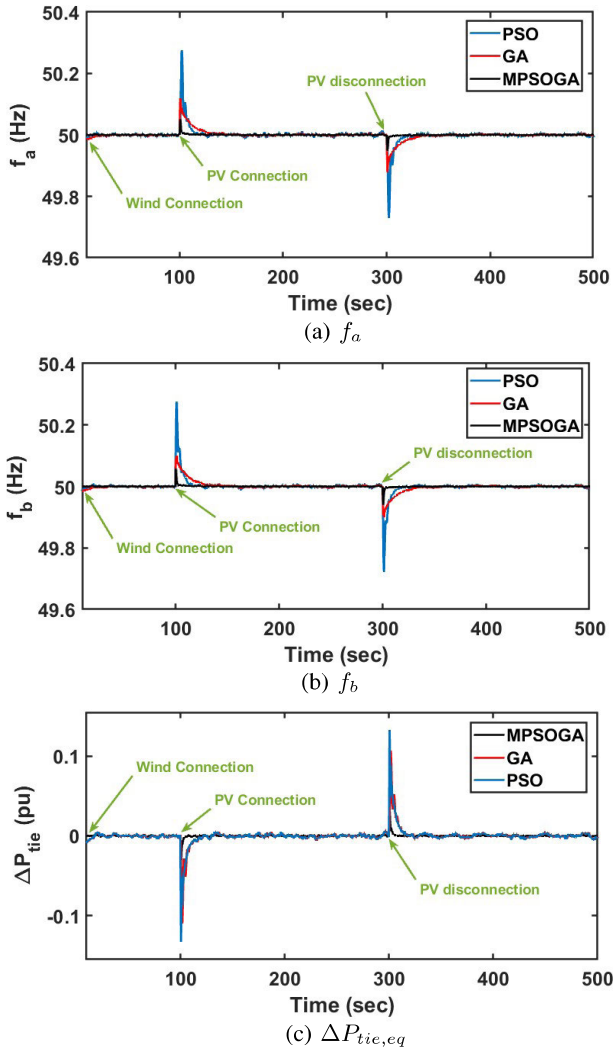

FIGURE 8. System dynamic response for scenario 1.

$t = 300$ s as shown in Fig. 7. Fig. 8 presents the performance of the two-area a and b, including the frequency deviations and the tie-line power. It is clear that the coordinated LFC based-TIDF controller and VIC based-TID SMES systems using the proposed MPSOGA algorithm can provide a satisfactory performance in restoring the system frequency against different disturbances, especially at the instants of connection/disconnection of PV generation. Whereas the designed controllers using the individual PSO and GA suffer from prolonged damped oscillations as shown in Fig. 8a, and Fig. 8b. Furthermore, the proposed hybrid MPSOGA method shows its ability to damp out the tie-line power oscillations compared to the others as depicted in Fig. 8c. It is also found that by adopting MPSOGA technique, the frequency and tie-line power transient response are enhanced with lower settling time compared to the other algorithms as summarized in Table. 3, wherein the maximum overshoot (MO) and the settling time (ST) are measured for the step changes at time slice of 100-200 s for this scenario. In addition, the MPSOGA technique have smooth curves with a faster convergence rate more than the conventional PSO and GA as shown in Fig. 9.

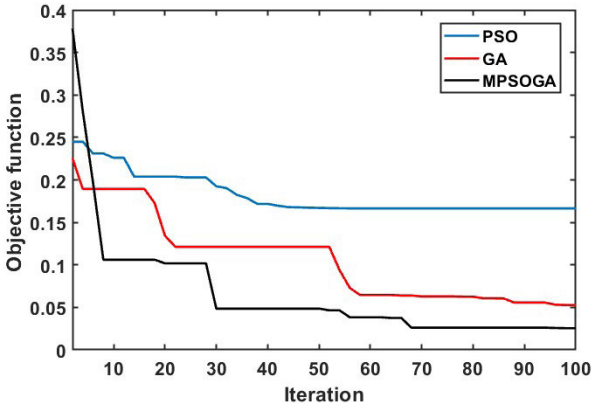

FIGURE 9. Convergence curve at scenario 1.

B. SCENARIO 2: LOAD STEP CHANGES

The effectiveness of the proposed cooperative VIC based-TID SMES and LFC base-TIDF using the new MPSOGA technique is tested at the extreme case of multi-step load variation. Whereas, the impact of high fluctuated wind and PV generations are also considered in this scenario. The profile for these scenarios for loads and generation are described in Fig. 10. The frequency deviation and the tie-line power responses of the studied system with the proposed controllers are shown in Fig. 11. It can be seen that the hybrid MPSOGA confirmed its robustness compared to conventional PSO and GA methods. The MPSOGA-based design can suppress the frequency fluctuations in areas a and b to a very low values in terms of MO and maximum undershoot as shown in Fig. 11a, and Fig. 11b and with minimum settling time as seen in Table. 3. In addition, the proposed MPSOGA-based design provides the best performance regarding mitigating the tie-line power oscillations compared to other methods as seen in Fig. 11c. Moreover, the proposed algorithm has a fast convergence rate compared to the other algorithms as shown in Fig. 12.Therefore, the proposed cooperative controllers based MPSOGA design is successful in adjusting the frequency and tie-line power to their normal values in all four stages of this multi-step load scenario. Fast charge/discharge process of the output power via SMES device, and proper mitigation of fast fluctuations represent the main features of the proposed MPSOGA design compared with the PSO and GA methods. Fig. 12 shows the superiority of the proposed MPSOGA in the convergence rate compared to the other conventional techniques.

C. SCENARIO 3: DISCONNECTION OF HVDC TIE-LINE

This scenario is tested to check the performance of the proposed cooperative controllers based-MPSOGA technique under all circumstances of multi-area. The different two-area interconnection is tested in the case of the HVDC connection is lost.Fig. 13a, and Fig. 13b show that utilizing the coordinated control based-MPSOGA design provides the

TABLE 3. Maximum overshoot (MO) and settling time (ST) for the different scenarios.

Scenario	Algorithm	Δf_a		Δf_b		$\Delta P_{tie,eq}$	
		MO	ST (sec)	MO	ST (sec)	MO	ST (sec)
No. 1 (at 100 sec)	GA	0.12	45	0.098	48	0.11	45
	PSO	0.275	35	0.276	34	0.132	42
	MPSOGA	0.051	15	0.057	20	0.029	10
No. 2 (at 400 sec)	GA	0.135	35	0.129	37	0.191	23
	PSO	0.428	44	0.290	48	0.237	22
	MPSOGA	0.041	6	0.081	15	0.064	10
No. 3 (at 400 sec)	GA	0.223	33	0.223	35	0.286	25
	PSO	0.637	42	0.429	45	0.359	29
	MPSOGA	0.167	15	0.141	25	0.111	12
No. 4 (at 400 sec)	GA	0.277	32	0.272	35	0.103	17
	PSO	1.015	40	0.657	42	0.343	28
	MPSOGA	0.139	20	0.070	8	0.065	15
No. 5 (at 100 sec)	GA	0.061	42	0.062	40	0.078	23
	PSO	0.173	48	0.115	20	0.101	25
	MPSOGA	0.040	25	0.030	16	0.023	9

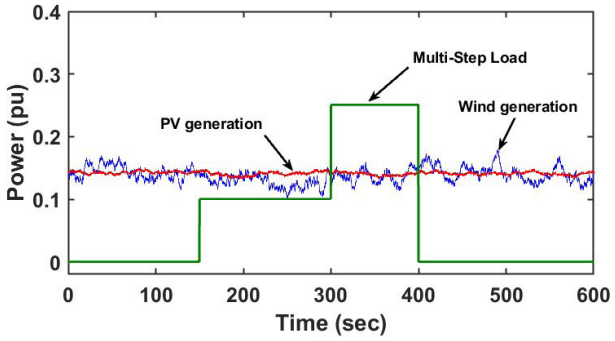

FIGURE 10. Generation and load profiles.

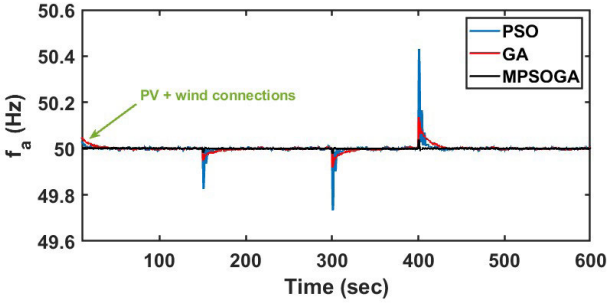

(a) f_a

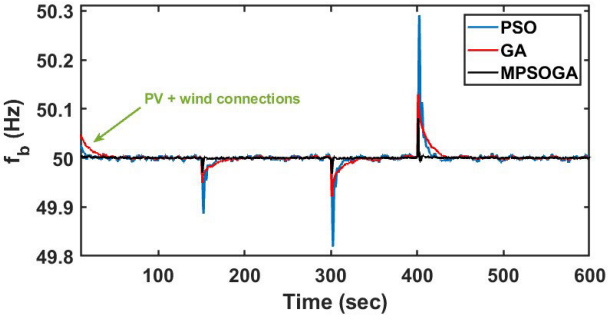

(b) f_b

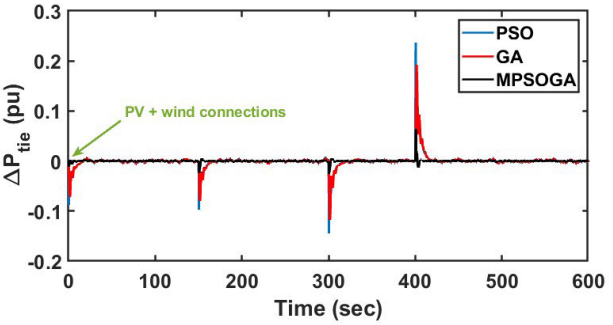

(c) $\Delta P_{tie,eq}$

FIGURE 11. System dynamic response at scenario 2.

capability to suppress the peak overshoot, peak undershoot, and oscillations of frequency deviations in areas a and b with fast settled transient response compared to the GA and PSO algorithms as mentioned in Table. 3. Furthermore, it is observed from Fig. 13c that the tie-line power based only on the HVAC tie-line has shorter settling time and smaller overshoot/undershoot using the proposed MPSOGA-based controller design than the other traditional meta-heuristic algorithms. On the other side, Fig. 14 shows the effective performance of the hybrid MPSOGA as ISE converges smoothly to its minimum values without fluctuations. Whereas, the GA suffers from a premature convergence, caused by particles stagnating around local optima, and PSO meanwhile suffers from excessively slow rate.

D. SCENARIO 4: ROBUSTNESS ANALYSIS

To investigate the performance of the proposed controllers, a more drastic scenario is conducted based on varying system physical parameters. The system parameters are varied as follows: $H = -50\%$; $D = +20\%$; $T_g = +30\%$; $T_t = -25\%$; $T_{SMES} = +35\%$ with the same conditions of scenario 2. Fig. 15 proves the robustness of the proposed MPSOGA-based design with theses sever changes in system uncertainties by successfully treating this contingency. Whereas, the PSO-based design has shown severe change along the search process, which may lead to unstable solution in damping frequency oscillations and the fluctuations in the tie-line power. The GA-based design has shown better

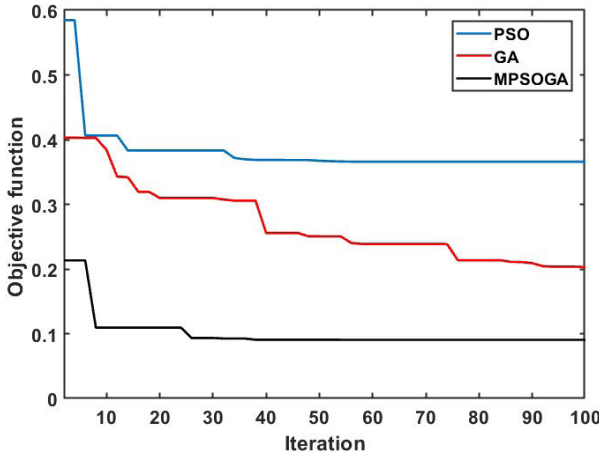

FIGURE 12. Convergence curve at scenario 2.

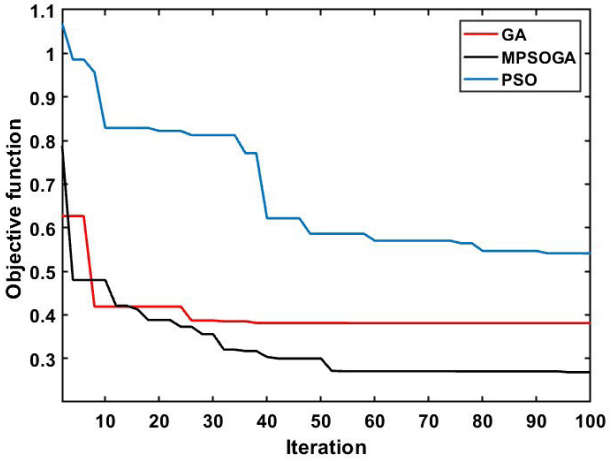

FIGURE 14. Convergence curve at scenario 3.

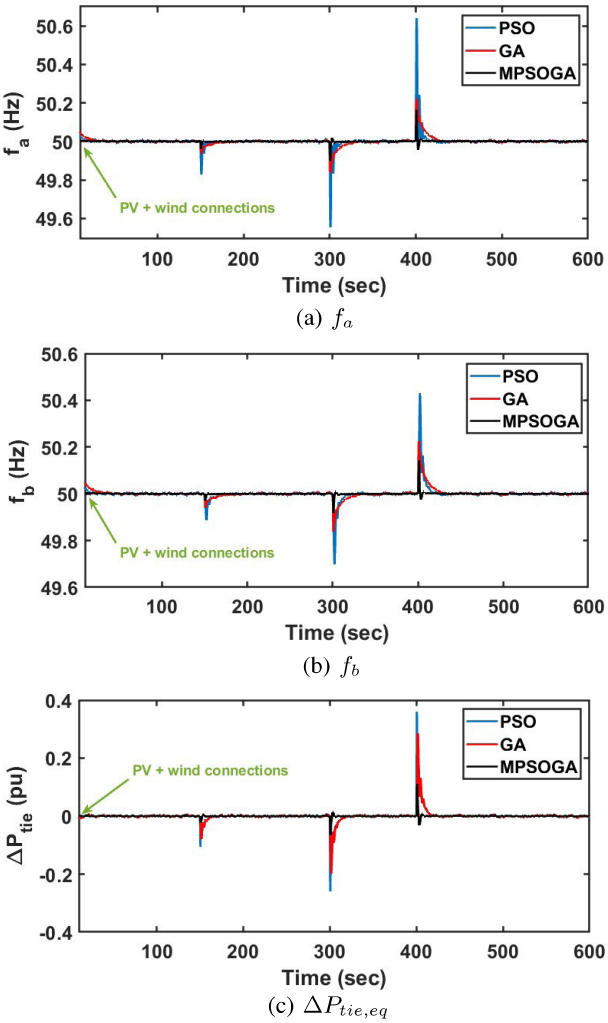

FIGURE 13. System dynamic response with HVDC failure at scenario 3.

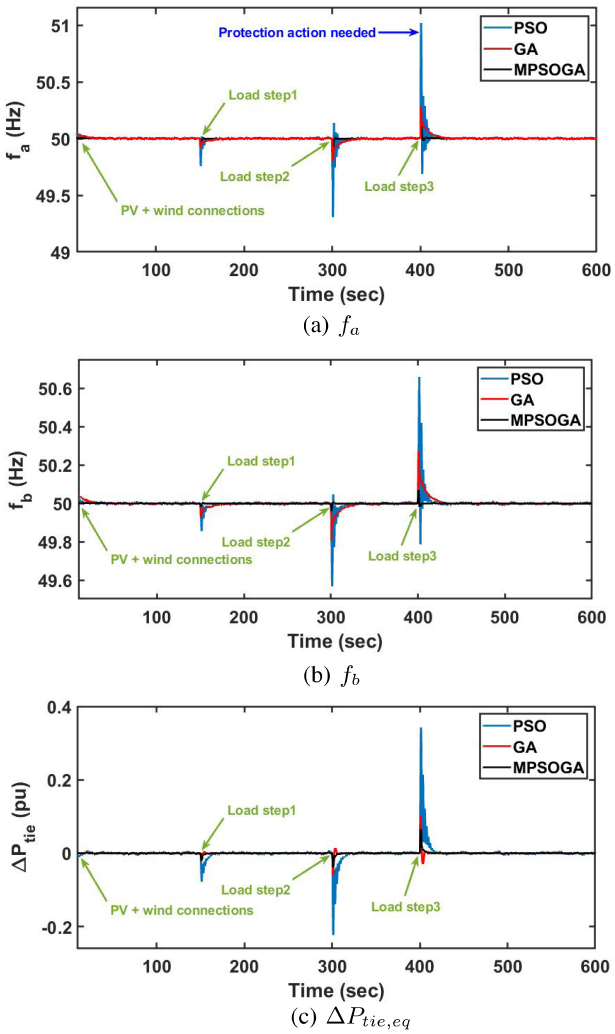

FIGURE 15. System dynamic response with system parameters variations at scenario 4.

performance than the PSO for dealing with the parameters variations. Furthermore, Table. 3 shows that the MPSOGA method has a lower value of settling time than GA and PSO algorithms. From another side, the proposed hybrid MPSOGA technique has lower sensitivity and more stable response dealing with a more severe case of system parameters variation than the other algorithms. Therefore, it can be manifested that the proposed MPSOGA provides superior robustness and effectiveness algorithm with the proposed

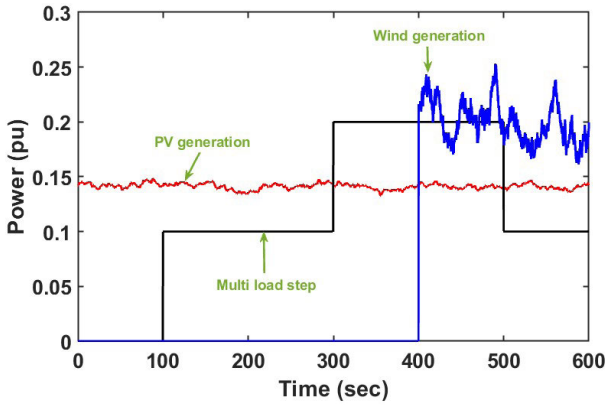

FIGURE 16. Power generation and load profiles.

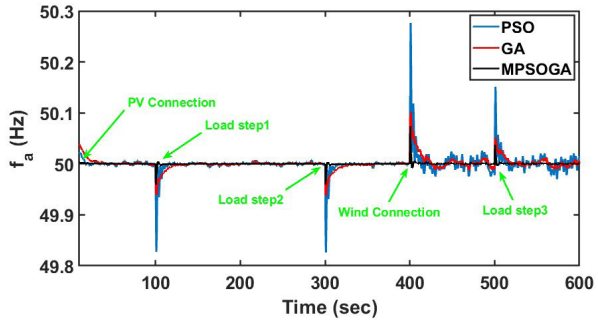

(a) f_a

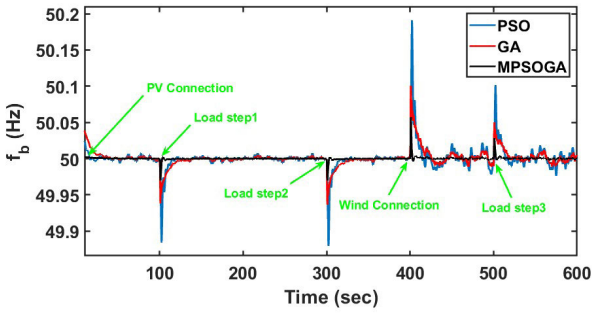

(b) f_b

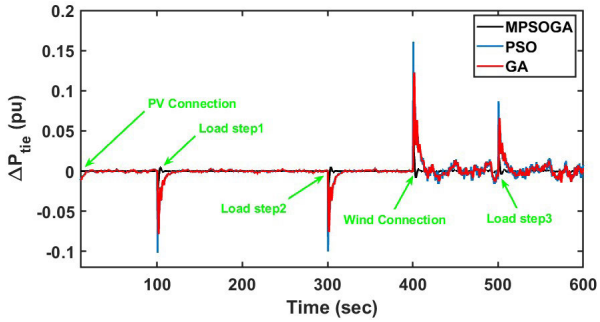

(c) $\Delta P_{tie,eq}$

FIGURE 17. System dynamic response with high wind penetration at scenario 5.

cooperative VIC and Tilt based-controllers over the other comparative methods.

E. SCENARIO 5: HIGH WIND POWER PENETRATION

In this scenario, the system under study is tested under extreme disturbances conditions of high wind power penetration and highly residential and industrial loads variations. The power fluctuations of the high wind and PV penetration and loads are shown in Fig. 16. The proposed cooperative controllers provided a perfect performance in diminishing the frequency and tie-power deviations from high wind penetrations and load variations in each area. Fig. 17a, Fig. 17b, and Fig. 17c show that the new hybrid MPSOGA proved its ability in suppressing the power and frequency fluctuations in areas a and b to a very small values with very fast response especially at severe instants of load add/shed at 300 sec and 500 sec, and wind power connection at 400 sec, respectively. These severe disturbances instants show the superiority of the proposed MPSOGA over the other conventional optimization techniques.

TABLE 4. ISE comparison between the various optimization methods.

Scenario	Optimization Methods		
	PSO	GA	MPSOGA
1	0.1792	0.0723	0.0376
2	0.3758	0.2163	0.0983
3	0.5486	0.3867	0.2785
4	0.7254	0.2981	0.1564
5	0.2156	0.0985	0.0265

F. PERFORMANCE COMPARISON

Table 4 shows the ISE estimations for the aforementioned tested four operating scenarios. The GA, PSO, and the proposed MPSOGA-based design are compared through the ISE index for each scenario. The proposed MPSOGA method provides overall improved performance for the control objectives through having lower ISE values than comparable algorithms. In scenario 1, the ISE of the proposed MPSOGA is 0.0376 compared to 0.0723, and 0.1792 for the GA and PSO methods, respectively. The other scenarios prove also the enhanced performance of the proposed MPSOGA-based design with the proposed cooperative TIDF LFC and VIC based-TID SMES methods.Therefore, the robustness and mitigation of various fluctuations represent the main features of the proposed design and control method over the traditional techniques.

VI. CONCLUSION

A new approach based on hybrid modified particle swarm optimization with genetic algorithm (MPSOGA) is proposed for solving LFC and VIC in an interconnected power system. Improving the learning capacity and the intergenerational transfer of information are the key features of the proposed MPSOGA process,in which they are integrated into sequential balanced stages to monitor the problem of exploration-exploitation. The ISE index is employed in the proposed method to represent the multi-objective function, including the frequency deviation at the two-area and the hybrid HVAC/HVDC tie-line powers. The proposed MPSOGA method has shown high robustness against the system parameters uncertainty; The estimated ISE shows

that the proposed MPSOGA at renewable energy behavior scenario has ISE values of 52% and 20.98% of the GA, and PSO methods, respectively. Whereas, during muti-load stepping, the proposed MPSOGA has ISE values of 45.45% and 26.16% of the GA, and PSO methods, respectively. In addition, the proposed MPSOGA method possesses superior robustness against HVDC failure and system parameters variations.

REFERENCES

[1] S. M. Said, M. Aly, B. Hartmann, A. G. Alharbi, and E. M. Ahmed, "SMES-based fuzzy logic approach for enhancing the reliability of microgrids equipped with PV generators," *IEEE Access*, vol. 7, pp. 92059–92069, 2019.

[2] M. Aly, E. M. Ahmed, and M. Shoyama, "Thermal and reliability assessment for wind energy systems with DSTATCOM functionality in resilient microgrids," *IEEE Trans. Sustain. Energy*, vol. 8, no. 3, pp. 953–965, Jul. 2017.

[3] E. Rakhshani, P. Rodriguez, A. M. Cantarellas, and D. Remon, "Analysis of derivative control based virtual inertia in multi-area high-voltage direct current interconnected power systems," *IET Gener., Transmiss. Distrib.*, vol. 10, no. 6, pp. 1458–1469, Apr. 2016.

[4] J. Zhao, X. Lyu, Y. Fu, X. Hu, and F. Li, "Coordinated microgrid frequency regulation based on DFIG variable coefficient using virtual inertia and primary frequency control," *IEEE Trans. Energy Convers.*, vol. 31, no. 3, pp. 833–845, Sep. 2016.

[5] H. Zhao, Q. Yang, and H. Zeng, "Multi-loop virtual synchronous generator control of inverter-based DGs under microgrid dynamics," *IET Gener., Transmiss. Distrib.*, vol. 11, no. 3, pp. 795–803, Feb. 2017.

[6] S. D'Arco, J. A. Suul, and O. B. Fosso, "Small-signal modeling and parametric sensitivity of a virtual synchronous machine in islanded operation," *Int. J. Electr. Power Energy Syst.*, vol. 72, pp. 3–15, Nov. 2015.

[7] U. Tamrakar, D. Shrestha, M. Maharjan, B. Bhattarai, T. Hansen, and R. Tonkoski, "Virtual inertia: Current trends and future directions," *Appl. Sci.*, vol. 7, no. 7, p. 654, Jun. 2017.

[8] T. Kerdphol, M. Watanabe, Y. Mitani, and V. Phunpeng, "Applying virtual inertia control topology to SMES system for frequency stability improvement of low-inertia microgrids driven by high renewables," *Energies*, vol. 12, no. 20, p. 3902, Oct. 2019.

[9] J. Liu, Y. Miura, and T. Ise, "Comparison of dynamic characteristics between virtual synchronous generator and droop control in inverter-based distributed generators," *IEEE Trans. Power Electron.*, vol. 31, no. 5, pp. 3600–3611, May 2016.

[10] J. Van De Vyver, J. D. M. De Kooning, B. Meersman, L. Vandevelde, and T. L. Vandoorn, "Droop control as an alternative inertial response strategy for the synthetic inertia on wind turbines," *IEEE Trans. Power Syst.*, vol. 31, no. 2, pp. 1129–1138, Mar. 2016.

[11] D. Chen, Y. Xu, and A. Q. Huang, "Integration of DC microgrids as virtual synchronous machines into the AC grid," *IEEE Trans. Ind. Electron.*, vol. 64, no. 9, pp. 7455–7466, Sep. 2017.

[12] T. Kerdphol, F. S. Rahman, Y. Mitani, M. Watanabe, and S. Küfeoğlu, "Robust virtual inertia control of an islanded microgrid considering high penetration of renewable energy," *IEEE Access*, vol. 6, pp. 625–636, 2018.

[13] A. Abu-Siada and S. Islam, "Application of SMES unit in improving the performance of an AC/DC power system," *IEEE Trans. Sustain. Energy*, vol. 2, no. 2, pp. 109–121, Apr. 2011.

[14] S. Nomura, H. Tsutsui, S. Tsuji-Iio, and R. Shimada, "Flexible power interconnection with SMES," *IEEE Trans. Appl. Supercond.*, vol. 16, no. 2, pp. 616–619, Jun. 2006.

[15] K. Mentesidi, R. Garde, M. Aguado, and E. Rikos, "Implementation of a fuzzy logic controller for virtual inertia emulation," in *Proc. Int. Symp. Smart Electr. Distrib. Syst. Technol. (EDST)*, Sep. 2015, pp. 606–611.

[16] T. Kerdphol, F. Rahman, Y. Mitani, K. Hongesombut, and S. Küfeoğlu, "Virtual inertia control-based model predictive control for microgrid frequency stabilization considering high renewable energy integration," *Sustainability*, vol. 9, no. 5, p. 773, May 2017.

[17] H. Ali, G. Magdy, B. Li, G. Shabib, A. A. Elbaset, D. Xu, and Y. Mitani, "A new frequency control strategy in an islanded microgrid using virtual inertia control-based coefficient diagram method," *IEEE Access*, vol. 7, pp. 16979–16990, 2019.

[18] H. Bevrani, M. R. Feizi, and S. Ataee, "Robust frequency control in an islanded microgrid: H_∞ and μ-synthesis approaches," *IEEE Trans. Smart Grid*, vol. 7, no. 2, pp. 706–717, Mar. 2016.

[19] T. Kerdphol, F. Rahman, and Y. Mitani, "Virtual inertia control application to enhance frequency stability of interconnected power systems with high renewable energy penetration," *Energies*, vol. 11, no. 4, p. 981, Apr. 2018.

[20] N. Pathak, A. Verma, T. S. Bhatti, and I. Nasiruddin, "Modeling of HVDC tie links and their utilization in AGC/LFC operations of multiarea power systems," *IEEE Trans. Ind. Electron.*, vol. 66, no. 3, pp. 2185–2197, Mar. 2019.

[21] N. R. Babu and L. C. Saikia, "Automatic generation control of a solar thermal and dish-stirling solar thermal system integrated multi-area system incorporating accurate HVDC link model using crow search algorithm optimised FOPI minus FODF controller," *IET Renew. Power Gener.*, vol. 13, no. 12, pp. 2221–2231, Sep. 2019.

[22] S. Oshnoei, A. Oshnoei, A. Mosallanejad, and F. Haghjoo, "Contribution of GCSC to regulate the frequency in multi-area power systems considering time delays: A new control outline based on fractional order controllers," *Int. J. Electr. Power Energy Syst.*, vol. 123, Dec. 2020, Art. no. 106197.

[23] R. K. Sahu, S. Panda, A. Biswal, and G. T. C. Sekhar, "Design and analysis of tilt integral derivative controller with filter for load frequency control of multi-area interconnected power systems," *ISA Trans.*, vol. 61, pp. 251–264, Mar. 2016.

[24] A. Delassi, S. Arif, and L. Mokrani, "Load frequency control problem in interconnected power systems using robust fractional PI λ d controller," *Ain Shams Eng. J.*, vol. 9, no. 1, pp. 77–88, Mar. 2018.

[25] Y. Arya, "A new optimized fuzzy FOPI-FOPD controller for automatic generation control of electric power systems," *J. Franklin Inst.*, vol. 356, no. 11, pp. 5611–5629, Jul. 2019.

[26] M. Gheisarnejad and M. H. Khooban, "Design an optimal fuzzy fractional proportional integral derivative controller with derivative filter for load frequency control in power systems," *Trans. Inst. Meas. Control*, vol. 41, no. 9, pp. 2563–2581, Jan. 2019.

[27] Y. Arya, "Improvement in automatic generation control of two-area electric power systems via a new fuzzy aided optimal PIDN-FOI controller," *ISA Trans.*, vol. 80, pp. 475–490, Sep. 2018.

[28] F. Daneshfar and H. Bevrani, "Multiobjective design of load frequency control using genetic algorithms," *Int. J. Electr. Power Energy Syst.*, vol. 42, no. 1, pp. 257–263, Nov. 2012.

[29] H. Shayeghi, A. Jalili, and H. A. Shayanfar, "Multi-stage fuzzy load frequency control using PSO," *Energy Convers. Manage.*, vol. 49, no. 10, pp. 2570–2580, Oct. 2008.

[30] T. K. Mohapatra and B. K. Sahu, "Design and implementation of SSA based fractional order PID controller for automatic generation control of a multi-area, multi-source interconnected power system," in *Proc. Technol. Smart-City Energy Secur. Power (ICSESP)*, Mar. 2018, pp. 1–6.

[31] H. Gozde, M. C. Taplamacioglu, and İ. Kocaarslan, "Comparative performance analysis of artificial bee colony algorithm in automatic generation control for interconnected reheat thermal power system," *Int. J. Electr. Power Energy Syst.*, vol. 42, no. 1, pp. 167–178, Nov. 2012.

[32] B. Mohanty, S. Panda, and P. K. Hota, "Differential evolution algorithm based automatic generation control for interconnected power systems with non-linearity," *Alexandria Eng. J.*, vol. 53, no. 3, pp. 537–552, Sep. 2014.

[33] S. M. Abd-Elazim and E. S. Ali, "Load frequency controller design of a two-area system composing of PV grid and thermal generator via firefly algorithm," *Neural Comput. Appl.*, vol. 30, no. 2, pp. 607–616, Jul. 2018.

[34] S. A. Taher, M. H. Fini, and S. F. Aliabadi, "Fractional order PID controller design for LFC in electric power systems using imperialist competitive algorithm," *Ain Shams Eng. J.*, vol. 5, no. 1, pp. 121–135, Mar. 2014.

[35] H. M. Hasanien, "Whale optimisation algorithm for automatic generation control of interconnected modern power systems including renewable energy sources," *IET Gener., Transmiss. Distrib.*, vol. 12, no. 3, pp. 607–614, Feb. 2018.

[36] M. Raju, L. C. Saikia, and N. Sinha, "Automatic generation control of a multi-area system using ant lion optimizer algorithm based PID plus second order derivative controller," *Int. J. Electr. Power Energy Syst.*, vol. 80, pp. 52–63, Sep. 2016.

[37] R. K. Sahu, T. S. Gorripotu, and S. Panda, "Automatic generation control of multi-area power systems with diverse energy sources using teaching learning based optimization algorithm," *Eng. Sci. Technol., Int. J.*, vol. 19, no. 1, pp. 113–134, Mar. 2016.

[38] C. K. Shiva and V. Mukherjee, "Automatic generation control of multi-unit multi-area deregulated power system using a novel quasi-oppositional harmony search algorithm," *IET Gener., Transmiss. Distrib.*, vol. 9, no. 15, pp. 2398–2408, Nov. 2015.
[39] E. A. Mohamed, E. M. Ahmed, A. Elmelegi, M. Aly, O. Elbaksawi, and A.-A. A. Mohamed, "An optimized hybrid fractional order controller for frequency regulation in multi-area power systems," *IEEE Access*, vol. 8, pp. 213899–213915, 2020, doi: 10.1109/access.2020.3040620.
[40] R. J. Abraham, D. Das, and A. Patra, "Automatic generation control of an interconnected hydrothermal power system considering superconducting magnetic energy storage," *Int. J. Electr. Power Energy Syst.*, vol. 29, no. 8, pp. 571–579, Oct. 2007.
[41] S. Padhan, R. K. Sahu, and S. Panda, "Automatic generation control with thyristor controlled series compensator including superconducting magnetic energy storage units," *Ain Shams Eng. J.*, vol. 5, no. 3, pp. 759–774, Sep. 2014.
[42] S. M. Said, E. A. Mohamed, and B. Hartmann, "Coordination strategy for digital frequency relays and energy storage in a low-inertia microgrid," *J. Power Technol.*, vol. 99, no. 4, pp. 254–263, 2019.
[43] A. Zamani, S. M. Barakati, and S. Yousofi-Darmian, "Design of a fractional order PID controller using GBMO algorithm for load–frequency control with governor saturation consideration," *ISA Trans.*, vol. 64, pp. 56–66, Sep. 2016.
[44] J. Morsali, K. Zare, and M. T. Hagh, "Applying fractional order PID to design TCSC-based damping controller in coordination with automatic generation control of interconnected multi-source power system," *Eng. Sci. Technol., Int. J.*, vol. 20, no. 1, pp. 1–17, Feb. 2017.
[45] S. Sondhi and Y. V. Hote, "Fractional order PID controller for load frequency control," *Energy Convers. Manage.*, vol. 85, pp. 343–353, Sep. 2014.
[46] E. Mohamed, A.-A.-A. Mohamed, and Y. Mitani, "Genetic-moth swarm algorithm for optimal placement and capacity of renewable DG sources in distribution systems," *Int. J. Interact. Multimedia Artif. Intell.*, vol. 5, no. 7, p. 105, 2019.
[47] E. A. Mohamed, A. A. Mohamed, and Y. Mitani, "Hybrid GMSA for optimal placement and sizing of distributed generation and shunt capacitors," *J. Eng. Sci. Technol. Rev.*, vol. 11, no. 1, pp. 55–65, 2018.
[48] A. A. Mohamed. (2020). *MPSOGA: New Hybridization of Modified Associative Learning Immediate Memory Technique With GA*. [Online]. Available: https://uk.mathworks.com/matlabcentral/fileexchange/75560-mpsoga

AHMED ELMELEGI received the B.Sc. and M.Sc. degrees in electrical power engineering from Aswan University, Aswan, Egypt, in 2005 and 2019, respectively. He joined Upper Egypt Electricity Distribution Company, Ministry of Electricity and Renewable Energy, Aswan, in 2007. His current research interests include applied power electronics in renewable energy applications, multi-level inverters, and micro-grids.

EMAD A. MOHAMED received the B.Sc. and M.Sc. degrees in electrical power engineering from Aswan University, Aswan, Egypt, in 2005 and 2013, respectively, and the Ph.D. degree in electrical power engineering from the Kyushu Institute of Technology, Japan, in 2019.

He was a Demonstrator with the Department of Electrical Engineering, Aswan Faculty of Engineering, Aswan University, from November 2007 to August 2013, and an Assistant Lecturer from 2013 to 2015. He was a Research Student with Kyushu University, Japan, from April 2015 to October 2015. He has been an Assistant Professor since May 2019. He was in the Master Mobility Scholarship with the Faculté des Sciences et Technologies, Université de Lorraine, France–1. This scholarship was sponsored by FFEEBB ERASMUS MUNDUS. His current research interests include the applications of superconducting power devices, power system stability, and reliability and protection.

MOKHTAR ALY (Member, IEEE) received the B.Sc. and M.Sc. degrees in electrical engineering from Aswan University, Aswan, Egypt, in 2007 and 2012, respectively, and the Ph.D. degree from the Department of Electrical Engineering, Faculty of Information Science and Electrical Engineering, Kyushu University, Japan, in 2017.

In 2008, he joined the Department of Electrical Engineering, Aswan University, as an Assistant Lecturer, where he has been an Assistant Professor with the Faculty of Engineering, since 2017. He is currently a Postdoctoral Researcher with the Solar Energy Research Center (SERC-Chile), Universidad Técnica Federico Santa María, Chile. His current research interests include the reliability of power electronics systems especially in renewable energy applications, multi-level inverters, fault tolerant control, electric vehicles, and light emitting diode (LED) lamp drivers. He is also a member of the IEEE Power Electronics Society (PELS), IEEE Industrial Electronics Society (IES), and IEEE Power and Energy Society (PES).

EMAD M. AHMED (Senior Member, IEEE) received the B.Sc. and M.Sc. degrees from Aswan University, Egypt, in 2001 and 2006, respectively, and the Ph.D. degree from Kyushu University, Japan, in 2012.

He was with the Aswan Power Electronics Applications Research Center (APEARC), from 2012 to 2018. He is currently working as an Associate Professor with the Department of Electrical Engineering, Faculty of Engineering, Aswan University. Moreover, he is on a leave at the Faculty of Engineering, Jouf University, Saudi Arabia. His current research interests include applied power electronics, especially in renewable energy applications, micro-grids, fault tolerant control, and battery management systems. He is a member of the IEEE Power Electronics Society (PELS), the IEEE Industrial Electronics Society (IES), and the IEEE Power and Energy Society (PES).

AL-ATTAR ALI MOHAMED received the B.Sc., M.Sc., and Ph.D. degrees in electrical engineering from Aswan University, Aswan, Egypt, in 2010, 2013, and 2017, respectively. He is currently an Assistant Professor with the Department of Electrical Engineering, Faculty of Engineering, Aswan University. His research interests include the analysis and design of power systems, optimization and controls, renewable energy applications, micro-grids, electric vehicles, and energy storage systems.

OSAMA ELBAKSAWI received the B.Sc. degree (Hons.) in electrical engineering from the Faculty of Engineering, Suez Canal University, Egypt, in 1996, and the M.Sc. and Ph.D. degrees in power and electrical machines from the Suez Canal University, in 2002 and 2009, respectively. From 2010 to 2014, he worked as an Assistant Professor in electrical engineering with the Faculty of Engineering, Port Said University. Since 2014, he has been an Assistant Professor with the College of Engineering, Jouf University. His research interests include power system and electrical machines, which can be classified into the following topics: control of power system, different optimization algorithms, load frequency control, micro-grid systems, drive systems and renewable energy conversion for PV, and wind systems.